Magnetic Properties and Structural Transitions of Orthorhombic Fluorite-Related Compounds Ln_3MO_7

(*Ln* = Rare Earths, *M* = Transition Metals)

Makoto Wakeshima and Yukio Hinatsu

Division of Chemistry, Graduate School of Science, Hokkaido University, Sapporo 060-0810, Japan

Abstract

Magnetic properties and structural transitions of ternary rare-earth transition-metal oxides Ln_3MO_7 (*Ln* = rare earths, *M* = transition metals) were investigated. In this study, we prepared a series of molybdates Ln_3MoO_7 (*Ln* = La ~ Gd). They crystallize in an orthorhombic superstructure of cubic fluorite with space group $P2_12_12_1$, in which Ln^{3+} ions occupy two different crystallographic sites (the 8-coordinated and 7-coordinated sites). All of these compounds show a phase transition from the space group $P2_12_12_1$ to *Pnma* in the temperature range between 370 and 710 K. Their magnetic properties were characterized by magnetic susceptibility measurements from 1.8 to 400 K and specific heat measurements from 0.4 K to 400 K. Gd_3MoO_7 shows an antiferromagnetic transition at 1.9 K. Measurements of the specific heat for Sm_3MoO_7 and the analysis of the magnetic specific heat indicate a “two-step” antiferromagnetic transition due to the ordering of Sm magnetic moments in different crystallographic sites, i.e., with decreasing temperature, the antiferromagnetic ordering of the 7-coordinated Sm ions occur at 2.5 K, and then the 8-coordinated Sm ions order at 0.8 K. The results of Ln_3MoO_7 were compared with the magnetic properties and structural transitions of Ln_3MO_7 (*M* = Nb, Ru, Sb, Ta, Re, Os, or Ir).

1. Introduction

Ternary metal oxides of general formula Ln_3MO_7 (*Ln* is a rare earth element; *M* is a pentavalent transition element such as Nb, Mo, Ru, Sb, Ta, Re, Os, or Ir) have been intensively studied. They have an ordered, defect-fluorite structure. The relationship to the fluorite structure is as follows. The fluorite unit cell for oxides has the composition $M^{4+}{}_4O_8$. If the four tetravalent metal ions are replaced by three trivalent ions (*Ln*) and one pentavalent ion (*M*), one oxide vacancy is formed per fluorite cell. Due to significant differences in radii between the Ln^{3+} and M^{5+} ions, cation ordering occurs on the metal sites and the oxide-vacancy orders on the anion sites. In 1979, Rossell first determined the crystal structure of an orthorhombic La_3NbO_7 [1]. The M^{5+} ion is coordinated with six oxygen ions, forming a MO_6 octahedron. These octahedra share corners forming one-dimensional chains which are oriented along the *c*-axis. A variety of the space groups such as *Pnma*, *Cmcm*, $P2_12_12_1$, $C222_1$, and $P2_1nb$ has been proposed for the Ln_3MO_7. Due to this unique crystal structures and possible related magnetic properties, many studies have been performed [2-41], especially for the magnetic properties of compounds containing Ru^{5+} ion at the *M*-site because of its largest possible spin (S = 3/2) [5-13]. However, there was scant evidence for the expected one-dimensionality in the magnetic susceptibility.

Another topic for Ln_3MO_7 is that detailed magnetic and thermal investigations on the ruthenium-, iridium- and osmium-containing members of the Ln_3MO_7 family show low-temperature structural phase transitions [9-11, 13, 14, 19, 26, 30, 31, 35-38, 40, 41]. However, the-low temperature structures are, in most cases, not known, or different structures were presented for the same compounds.

We have paid our attention on the *M* = Mo compounds. Prevost-Czeskleba first reported that Ln_3MoO_7 (*Ln* = La, Pr, Nd, Sm, Eu) crystallized in an orthorhombic phase with space group *Cmcm*

from their powder X-ray diffraction measurements [27]. Later, Greedan and Gougeon prepared single crystals of Ln_3MoO_7 (*Ln* = La, Pr) and performed their X-ray diffraction measurements [28, 29]. These compounds crystallize in the orthorhombic space group $P2_12_12_1$. They studied the electronic and thermal properties of La_3MoO_7 by magnetic susceptibility, electric resistivity, and neutron diffraction measurements as a function of temperature. The magnetic susceptibility was quite complex. The main feature was a broad maximum at 655 K which was interpreted as due to intra-chain spin corrections of the Mo^{5+} ions. Several other anomalies were observed at 483, 140, and 100 K. Then, we prepared a series of $LnMoO_7$ compounds (*Ln* = La, Pr, Nd, Sm, and Eu) and reported their crystal structures and magnetic properties [30]. The structures at room temperature were analyzed with the space group $P2_12_12_1$. The differential scanning calorimetry (DSC) measurements indicated that the phase-transition occurs for any Ln_3MO_7 compound in the temperature range between 370 and 710 K. However, we could not determine the crystal structure above the phase-transition temperature. Very recently, Gougeon et al. determined the crystal structures of Ce_3MoO_7 and Sm_3MoO_7 by using their single crystals [33, 39].

In this study, we extended the preparation of Ln_3MoO_7 compounds from *Ln* = La to Gd. Through high-temperature X-ray diffraction measurements, their crystal structures above the phase-transition were determined. In order to elucidate magnetic properties of these Ln_3MoO_7 compounds, the magnetic susceptibility measurements from 1.8 to 400 K and the specific heat measurements from 0.4 to 400 K were performed. The results of the magnetic properties and structural transitions for Ln_3MoO_7 were compared with those for Ln_3MO_7 (*M* = Nb, Ru, Sb, Ta, Re, Os, or Ir).

2. Experimental

2.1. Sample preparation

As starting materials, rare earth oxides Ln_2O_3 (*Ln* = La, Nd, Sm-Gd), MoO_2, and MoO_3 were used. For the preparation of *Ln* = Pr compound, Pr_6O_{11} was used as the starting material. To obtain sesquioxide Pr_2O_3, the Pr_6O_{11} was reduced in a flowing H_2 atmosphere at 900 °C for a day. For La_2O_3 and Nd_2O_3, they absorb moisture in air and easily form rare earth hydroxides $Ln(OH)_3$. Therefore, they were dried at 1173 K for 24 h before use. These starting materials were weighed in an appropriate metal ratio and were ground in an agate mortar. The mixtures were pressed into pellets and then sealed in an evacuated platinum tube. They were heated at 1200 °C for 12 h, and then cooled down to room temperature. After regrinding and repelleting, the same heating procedure was repeated again. For the preparation of Ln = Gd compound, the pelletized starting materials were sealed in a platinum tube, and were heated at 1350 °C for 3 h × 2. In the first stage of sample preparations, very small amounts of impurities remained in the desired compound because of the evaporation of Mo oxides; they were unreacted starting materials Gd_2O_3. In order to remove these impurities, the sample was washed with diluted hydrochloric acid. After this treatment, a single-phase Gd_3MoO_7 compound could be obtained.

2.2. X-ray diffraction analysis

Powder X-ray diffraction profiles were measured using a Rigaku Multi-Flex diffractometer with Cu-*Kα* radiation (λ = 1.5406 Å) equipped with a curved graphite monochromator. The data were collected by step- scanning in the angle range of $10° \leq 2\theta \leq 120°$ at a 2θ step-size of 0.02°. The X-ray diffraction data were analyzed by the Rietveld technique, using the programs RIETAN2000 [42].

2.3. Magnetic susceptibility measurements

The temperature-dependence of the magnetic susceptibility was measured in an applied field of 0.1 T over the temperature range of 1.8 K $\leq T \leq$ 400 K, using a SQUID magnetometer (Quantum Design, MPMS5S). The susceptibility measurements were performed under both zero-field-cooled (ZFC) and field-cooled (FC) conditions. The former was measured upon heating the sample to 400 K under the applied magnetic field of 0.1 T after zero-field cooling to 1.8 K. The latter was measured upon cooling the sample from 400 to 1.8 K at 0.1 T.

2.4. Specific heat measurements

Specific heat measurements were performed using a relaxation technique by a commercial heat capacity measuring system (Quantum Design, PPMS) in the temperature range of 0.4-400 K. The sintered sample in the form of a pellet was mounted on a thin alumina plate with Apiezon for better thermal contact.

2.5. Differential scanning calorimetry measurements

The DSC measurements were carried out under flowing Ar gas atmosphere over the temperature range 300-800 K using DSC 200 (Seiko, Japan). The heating rate was 5 K/min.

3. Results and discussion

3.1. Preparation and crystal structure

In this study, we could obtain a new compound Gd_3MoO_7 as a single phase. Figure 1 shows the powder X-ray diffraction profile for Gd_3MoO_7 measured at room temperature. The diffraction pattern is quite similar to those for *Ln* = La ~ Eu compounds. Their crystal structures have been elucidated and they are orthorhombic with space group $P2_12_12_1$ [28-30, 33]. We have performed refinement of the crystal structure with the same space group. The results of the Rietveld analysis show that Gd_3MoO_7 are isomorphous with Ln_3MoO_7 (*Ln* = La~Eu). Table 1 lists the crystallographic data for Gd_3MoO_7, and Figure 2 (a) shows its crystal structure. The structural feature of Gd_3MoO_7 is the occurrence of infinite single chains of tilted corner-linked MoO_6 octahedra running parallel to the b axis. These MoO_6 chains alternate with rows of edge-shared $Gd(1)O_8$ pseudo-cubes to form slabs parallel to the *ab*-plane. The slabs are separated by the Gd(2) and Gd(3) cations, which are seven-coordinated by O atoms forming highly distorted pentagonal bipyramids. Gall and Gougeon found that the average value of Mo-O distances within the MoO_6 octahedra decreases from 1.981 to 1.966 Å when the Ln^{3+} ionic radius decreases from La to Sm [39]. The average Mo-O distance determined for Gd_3MoO_7 is 1.953 Å, which follows the above-mentioned relationship. They also pointed out that a slight decrease in the Mo-O(5)-Mo angle was observed when the Ln^{3+} ionic radius decreases, and it changes from 149.1º (*Ln* = La) to 146.6º (*Ln* = Sm). The value of Gd_3MoO_7 is 146.2º, which also follows the above-mentioned relationship. The MoO_6 octahedra and $Gd(1)O_8$ cubes in this $P2_12_12_1$ structure are obviously not so much regular. The Mo-O distances change from 1.81(2) to 2.04(3) Å. The Gd(1) cation has seven

oxygen atoms as its nearest neighbors at distances ranging between 2.29(3) and 2.71(2) Å and an eighth at 3.34(2) Å (Gd(1)-O(3)) which form a highly distorted cube. This distortion results from the rotation of the MoO_6 octahedra around the b-axis.

The results of the X-ray diffraction measurements show that any of the Ln_3MoO_7 compounds crystallizes in the orthorhombic space group $P2_12_12_1$ at room temperature. The DSC measurements indicate that the phase transition occurs for all Ln_3MoO_7 (*Ln* = La ~ Sm) compounds in the temperature range between 370 and 710 K and that the phase-transition temperature increases from La_3MoO_7 to Sm_3MoO_7. We performed high-temperature XRD measurements for La_3MoO_7 in the temperature range between 300 and 500 K. Figure 3 (a) shows the XRD profiles measured at 300 and 460 K, and Fig. 3 (b) depicts its low 2θ region. When the temperature was increased above 370 K, some weak diffraction lines (for example, the peaks at 2θ ~ 20º and 39º corresponding to the 1 0 2 (0 1 2) and 3 0 2 reflections, respectively) disappeared and the XRD profile was successfully refined with the space group *Pnma*. This space group is a supergroup of $P2_12_12_1$, and has been applied also for Ln_3NbO_7 (*Ln* = La, Pr, Nd) [2, 38]. Table 2 lists the structural parameters for La_3MoO_7. The high-temperature structure of La_3MoO_7 is illustrated in Fig. 2 (b). Two kinds of infinite chains are formed by corner-sharing MoO_6 octahedra and edge-sharing $La(1)O_8$ cubes, and the slabs consist of alternate chains, and 7-coordinated La(2) ions exist between the slabs. The MoO_6 octahedra and $La(1)O_8$ cubes in the *Pnma* structure are obviously much more regular than those in the $P2_12_12_1$ structure. In the former, the tilting of the MoO_6 chain is along the 001 direction with the tilting angle (Mo-O-Mo) of 152.6º, and in the latter, it is along the 100 direction with the tilting angles of 149.1º for La_3MoO_7 and 146.2º for Gd_3MoO_7.

Table 3 lists the room-temperature crystal structures for Ln_3MoO_7 and other Ln_3MO_7 compounds

(*M* = Nb, Ta, Sb, Re, Os, Ir, Ru). Structural studies on Ln_3TaO_7 compounds show that with decreasing the size of Ln^{3+} ion, the space group of the Ln_3TaO_7 compounds changes from *Cmcm* to $C222_1$ to *Fm*-3*m* [24]. For *Ln* = Nd and Ho compounds, two-phases coexist at room temperature. With increasing temperature, they changed to a single-phase compound with the space group *Cmcm* (for *Ln* = Nd) and $C2_12_12_1$ (for *Ln* = Ho). Similar change of the structure with increasing temperature and with decreasing the size of Ln^{3+} ions has been observed for diamagnetic *M* ions, i.e., M^{5+} = Nb^{5+}, Sb^{5+} [38, 40].

Figure 4 shows the variation of the structural phase transition temperatures of Ln_3MoO_7 against the ionic radius of Ln^{3+} in eight-coordination. The data for a series of Ln_3MO_7 (*M* = Re, Os, Ir, Ru) compounds are also shown in the same figure. These M^{5+} ions have a *d*-electron configuration ranging from d^1 to d^4, indicating that the Ln_3MO_7 compounds are magnetically active. For each of the five series of Ln_3MO_7 compounds, the structure transition temperatures decrease with increasing the ionic radius of Ln^{3+}, i.e., it is clear that the structure transition of Ln_3MO_7 is clearly influenced by the size of the Ln^{3+} cation. As the transition temperature increases with decreasing the ionic radius of Ln^{3+}, the transition is stress-induced and occurs with lattice contraction on cooling. Each transition temperature within a series is separated by approximately the same temperature interval except for the case of Ln_3MoO_7. The trend of the transition temperature against Ln^{3+} radius for Ln_3MoO_7 is different from those for Ln_3MO_7 (*M* = Ru, Re, Os, Ir). The reason for this may be related to the difference in their high-temperature structures, that is, the Ln_3MoO_7 exists in the *Pnma* structure, whereas the other Ln_3MO_7 (*M* = Ru, Re, Os, Ir) exists in the *Cmcm* structure.

3.2. Magnetic properties

3.2.1. General magnetic properties of Ln_3MoO_7

In the preceding paper, we briefly reported magnetic properties of Ln_3MoO_7 compounds [30]. In this study, we performed measurements of magnetic susceptibilities and specific heat for Gd_3MoO_7 and re-measured magnetic susceptibilities and specific heat of Sm_3MoO_7. Table 4 summarizes their results with the data reported by Greedan et al. [28] and Gall and Gougeon [39]. The La_3MoO_7 shows complex magnetic behavior at 150 and 380 K. Below these temperatures, there is a large difference in the temperature-dependence of the magnetic susceptibility measured under zero-field-cooled condition and under field-cooled condition [28, 30]. The magnitude of the susceptibility of La_3MoO_7 is much smaller than that expected by about a factor of 10^{-2} for a simple $S = 1/2$ paramagnet, and there is no Curie-Weiss regime in the experimental temperature range. Therefore, magnetic properties of Ln_3MoO_7 are mainly due to the magnetic behavior of Ln^{3+} ions in the compounds. The Nd_3MoO_7 and Gd_3MoO_7 show a clear antiferromagnetic transition at 2.5 and 1.9 K, respectively. From the susceptibility measurements, both Pr_3MoO_7 and Sm_3MoO_7 show the existence of magnetic anomaly at 8.0 and 2.5 K, respectively. Other compounds (*Ln* = Ce, Eu) are paramagnetic down to 1.8 K [30, 39]. The effective magnetic moments and the Weiss constants were determined in the Curie-Weiss law temperature region. For Sm_3MoO_7 and Eu_3MoO_7, the susceptibility does not obey the Curie-Weiss law because Sm^{3+} and Eu^{3+} ions show the well-known van Vleck paramagnetism [43].

3.2.2. Magnetic properties of Gd_3MoO_7

Figure 5 shows the temperature dependence of the magnetic susceptibility for Gd_3MoO_7 in the low temperature region. An antiferromagnetic transition has been observed at 1.9 K. There is no divergence between the ZFC and FC susceptibilities. The inset of Fig. 5 shows the reciprocal

susceptibility versus temperature curve and the Curie-Weiss fitting in the temperature range of 10 to 400 K. The effective magnetic moment of Gd_3MoO_7 is determined to be 14.06 (2) μ_B. From this value, the magnetic moment of each Gd^{3+} ion is calculated to be 8.12 (1) μ_B, which is a little larger than the moment of free Gd^{3+} ion (7.94 μ_B), indicating the magnetic contribution of Mo^{5+} ion.

In order to obtain the information on the low-temperature magnetic behavior, specific heat measurements were performed down to 0.4 K. Figure 6 (a) shows the temperature dependence of the specific heat divided by temperature (C_p/T) for Gd_3MoO_7. A clear λ-type specific heat anomaly has been observed at 1.9 K, which corresponds to the results by magnetic susceptibility measurements. To evaluate the magnetic contribution to the specific heat (C_{mag}), we have to subtract the contribution of lattice specific heat (C_{lat}) from the total specific heat ($C_{mag} = C_p - C_{lat}$). The lattice specific heat was estimated by using the data for La_3MoO_7 (the solid line of Fig. 6 (a)). From the temperature dependence of the magnetic specific heat, the magnetic entropy change for Gd_3MoO_7 (S_{mag}) is calculated by the relation $S_{mag} = \int (C_{mag}/T) dT$. Temperature dependences of the magnetic specific heat divided by temperature (C_{mag}/T) and the magnetic entropy change (S_{mag}) for Gd_3MoO_7 are shown in Fig. 6 (b). The total magnetic entropy change is ~ 34 J/mol K, and this value is a little smaller than the value of $3R \ln 8$ = 51.9 J/mol K (R: gas constant). One reason for this is that we do not include the magnetic specific heat below 0.4 K in the estimation of the magnetic entropy change. Anyway, the results indicate that all the Gd^{3+} ions contribute to the antiferromagnetic transition and that the ground state of the Gd^{3+} ions is still eight-degenerate ($^8S_{7/2}$) without crystal field splitting.

3.2.3. Low-temperature magnetic properties of Sm_3MoO_7

Measurements of the specific heat down to 0.4 K for Sm_3MoO_7 and the analysis of the magnetic

specific heat indicate a “two-step” antiferromagnetic transition due to the ordering of Mo magnetic moments in different crystallographic sites.

Figure 7 shows the temperature dependence of the magnetic susceptibility for Sm_3MoO_7 in the low temperature region. Small magnetic anomaly has been observed at 2.5 K, but the susceptibility increases with decreasing temperature below this temperature. There is no divergence between the ZFC and FC susceptibilities, even below this temperature. Figure 8 (a) shows the temperature dependence of the specific heat (C_p) for Sm_3MoO_7. A λ-type specific heat anomaly has been observed at 2.5 K, which corresponds to the results by magnetic susceptibility measurements. In addition, another λ-type specific heat anomaly has been found at 0.8 K, indicating the existence of another magnetic ordering at this temperature. The magnetic specific heat of Sm_3MoO_7 was estimated by subtracting the contribution of the lattice specific heat from the total specific heat in the same way as is the case for Gd_3MoO_7. The temperature dependences of the magnetic specific heat divided by temperature (C_{mag}/T) and the magnetic entropy change (S_{mag}) for Sm_3MoO_7 are shown in Fig. 8 (b). The magnetic specific heat below 0.4 K was extrapolated by the relation $C_{mag} \propto T^3$ from the spin-wave model for the antiferromagnet [44] (the dotted line of Fig. 8 (b)). The magnetic entropy change associated with the sum of the two magnetic anomalies (at 0.8 and 2.5 K) is determined to be 15.3 J/mol K. The Sm^{3+} ions in the Sm_3MoO_7 occupy two crystallographic sites, the 8-coordinated Sm(1) site and 7-coordinated Sm(2) site, with the ratio 1:2. In both sites, the ground multiplet $^4I_{9/2}$ of the Sm^{3+} ion should be split into five Kramers doublets by the crystal field in the orthorhombic symmetry. At sufficiently low temperatures, only the lowest doublet of each Sm^{3+} ions needs to be considered. The observed value of magnetic entropy is close to $3R \ln 2 = 17.3$ J/mol K, which indicates that the ground doublets for three Sm^{3+} ions cause the

antiferromagnetic ordering.

As shown in Fig. 8, it is difficult to divide the magnetic entropy data into two anomalies. However, it is clear that the magnetic entropy change due to the magnetic anomaly at a higher temperature (2.5 K) is larger than that at a lower temperature (0.8 K), and the magnetic entropy seems to show a step-wise increase (Rln2 + 2Rln2) corresponding to two specific heat anomalies at 0.8 and 2.5 K, respectively. This experimental result suggests that the anomalies observed at 0.8 and 2.5 K are due to the antiferromagnetic ordering of Sm^{3+} ions independently in the 8-coordinated Sm(1) and 7-coordinated Sm(2) sites, respectively. Similar "two-step" antiferromagnetic transitions have been found in Ln_3TaO_7 (*Ln* = Nd, Tb) [24], Ln_3NbO_7 (Ln = Nd, Tb) [38], and Gd_3SbO_7 [40].

3.2.4. Comparison of the magnetic properties of Ln_3MoO_7 with those of Ln_3MO_7 (M = Nb, Ta, Sb, Re, Os, Ir, Ru)

Table 5 lists the magnetic properties of Ln_3MoO_7 with those of Ln_3MO_7 compounds (*M* = Nb, Ta, Sb, Re, Os, Ir, Ru). Since the pentavalent Nb, Ta, and Sb ions are diamagnetic, only the trivalent Ln ions contribute to the magnetic properties of Ln_3MO_7 compounds. Their magnetic properties are very similar. For example, any of the *Ln* = Nd compounds shows "two-step" antiferromagnetic transitions at 0.6 ~ 3.0 K. All *Ln* = Tb compounds order at 2.2 ~ 3.9 K. Other compounds such as *Ln* = Pr, Sm, Eu, Er, Tm, and Yb are paramagnetic. Although Ir^{5+} ions have $5d^2$ unpaired electrons, magnetic properties of Ln_3IrO_7 compounds are close to those of Ln_3MO_7 (*M* = Nb, Ta, Sb) compounds, that is, a *Ln* = Nd compound shows an antiferromagnetic ordering at almost the same temperature, 2.6 K, and other Ln_3IrO_7 (*Ln* = Pr, Sm, Eu) compounds are paramagnetic down to 1.8 K. It seems that Ir^{5+} ions do not contribute to the magnetic properties of Ln_3IrO_7 compounds. On the other hand, both Os^{5+} and Ru^{5+} ions

have the largest possible spin (S = 3/2) and any of the Ln_3MO_7 compounds containing these M^{5+} ions shows a variety of magnetic transitions at relatively high temperatures. Their magnetic properties are due to both Ln^{3+} and M^{5+} ions, and therefore could be modulated as a function of the electronic configuration of the Ln^{3+} ions. Magnetic properties of Ln_3MoO_7 compounds are not classified into any of the above mentioned two categories, and are unique, as described in this paper.

References

[1] H. J. Rossell, *J. Solid State Chem.*, **27**, 115-122 (1979).

[2] A. Kahn-Harari, L. Mazerrolles, D. Michel, and F. Robert, *J. Solid State Chem.*, **116**, 103-106 (1995).

[3] F. P. F. van Berkel and D. J. W. IJdo, *Mater. Res. Bull.*, **21**, 1103-1106 (1986).

[4] W. A. Groen, F. P. F. van Berkel, and D. J. W. IJdo, *Acta Crystallogr*. Sec. **C 43**, 2262-2264 (1986).

[5] P. Khalifah, R. W. Erwin , J. W. Lynn, Q. Huang, B. Batlogg, and R. J. Cava, *Phys. Rev.*, **B 60**, 9573-9578 (1999).

[6] P. Khalifah, Q. Huang, J. W. Lynn, R. W. Erwin, and R. J. Cava, *Mater. Res. Bull.*, **35**, 1-7 (2000).

[7] F. Wiss, N. P. Raju, A. S. Wills, and J. E. Greedan, *Inter. J. Inorg. Mater.*, **2**, 53-59 (2000).

[8] B.P.Bontchev, A.J.Jacobson, M.M.Gospodinov, V. Skumryev, V. N. Popov, B. Lorenz, R. L. Meng, A. P. Litvinchuk, and M.N. Iliev, *Phys. Rev*. **B. 62**, 12235-12240 (2000).

[9] D. Harada and Y. Hinatsu, *J. Solid State Chem.*, **158**, 245-253 (2001).

[10] D. Harada, Y. Hinatsu, and Y. Ishii, *J. Phys.: Condens. Matter*, **13**, 10825-10836 (2001).

[11] D. Harada and Y. Hinatsu, *J. Solid State Chem.*, **164**, 163-168 (2002).

[12] R. Lam, F. Wiss, and J. E. Greedan, *J. Solid State Chem.* **167**, 182-187 (2002).

[13] W. R. Gemmill, M. D. Smith, and H-C, zur Loye, *Inorg. Chem.*, **43**, 4254-4261 (2004).

[14] N. Ishizawa, K. Hiraga, D. du Boulay, H. Hibino, T. Ida, and S. Oishi, *Acta Cryst.*, **E62**, i13-i16 (2006).

[15] G. Wltschek, H. Paulus, I. Svoboda, H. Ehrenberg, and H. Fuess, *J.Solid State Chem.* **125**, 1-4

(1996).

[16] R. Lam, T. Langet, and J. E. Greedan, *J. Solid State Chem*. **171**, 317-323 (2002).

[17] Y. Hinatsu, M. Wakeshima, N. Kawabuchi, and N. Taira, *J. Alloys Compd*., **374**, 79-83 (2004).

[18] J. R. Plaisier, R. J. Drost, and D. J. W. IJdo, *J. Solid State Chem.* **169**, 189-198 (2002).

[19] W. R. Gemmill, M. D. Smith, Y. A. Mozharivsky, G. J. Miller, and H-C, zur Loye, *Inorg. Chem.*, **44**, 7047-7055 (2005).

[20] J. G. Allpress and H. J. Rossell, *J. Solid State Chem.*, **27**, 105-114 (1979).

[21] Y. Yokogawa, M. Yoshimura, and S. Somiya, *Mater. Res. Bull*., **22**, 1449-1456 (1987).

[22] Y. Yokogawa, M. Yoshimura, and S. Somiya, *Solid State Ionics*, **28**, 1250-1253 (1988).

[23] J. F. Vente, R. B. Helmholdt, and D. J. W. IJdo, *J. Solid State Chem*. **108**, 18-23 (1994).

[24] M. Wakeshima, H. Nishimine, and Y. Hinatsu, *J. Phys.: Condens. Matter*, **16**, 4103-4120 (2004).

[25] J. F. Vente and D. J. W. IJdo, *Mater. Res. Bull.*, **26**, 1255-1262 (1991).

[26] H. Nishimine, M. Wakeshima, and Y. Hinatsu, *J. Solid State Chem*., **177**, 739-744 (2004).

[27] H. Prevost-Czeskleba, *J. Less-Common Metals*, **127**, 117-124 (1987).

[28] J. E. Greedan, N. P. Raju, A. Wegner, P. Gougeon, and J. Padiou, *J. Solid State Chem*., **129**, 320-327 (1997).

[29] N. Barrier and P. Gougeon, *Acta Crystallogr.*, **E59**, i22-i24 (2003).

[30] H. Nishimine, M. Wakeshima, and Y. Hinatsu, *J. Solid State Chem*., **178**, 1221-1229 (2005).

[31] N. Ishizawa, K. Tateishi, S. Kondo, and T. Suwa, *Acta Crystalllogr*., **47**, 558-566 (2006).

[32] T. Fennell, S. T. Bramwell, and M. A. Green, *Can. J. Phys*., **79**, 1415-1419 (2001).

[33] N. Barrier, P. Gall, and P. Gougeon, *Acta Crystallogr*., **C63**, i102-i104 (2007).

[34] W. R. Gemmill, M. D. Smith, and H-C, zur Loye, *J. Chem*. Crystallogr, **37**, 793-795 (2007).

[35] N. Ishizawa, T. Suwa, K. Tateishi, and J. R. Hester, *Acta Cryst*., **C63**, i43-i46 (2007).

[36] N. Ishizawa, T. Suwa, and K. Tateishi, *Acta Cryst*., **E63**, i163 (2007).

[37] N. Ishizawa, K. Tateishi, S. Kondo, and T. Suwa, *Inorg. Chem.*, **47**, 558-566 (2008).

[38] Y. Doi, Y. Harada, and Y. Hinatsu, *J. Solid State Chem.*, **182**, 709-715 (2009).

[39] P. Gall and P. Gougeon, *J. Solid State Chem*., **182**, 1035-1039 (2009).

[40] Y. Hinatsu, H. Ebisawa, and Y. Doi, *J. Solid State Chem.*, **182**, 1694-1699 (2009).

[41] L. Cai, S. Denev, V. Gopalan, and J. Nino, *J. Am. Ceram. Soc*., **93**, 875-880 (2010).

[42] F. Izumi and T. Ikeda, *Mater. Sci. Forum*, **198**, 321-324 (2000).

[43] J. H. van Vleck, “Theory of Electric and Magnetic Susceptibilities”, Oxford, Clarendon, 1932.

[44] S. J. Joshua and A. P. Cracknell, *Phys. Lett*., **A28**, 562-563 (1969).

Figure captions

Fig. 1 Powder X-ray diffraction profiles for Gd_3MoO_7. The calculated and observed profiles are shown on the top solid line and cross markers, respectively. The vertical marks in the middle show positions calculated for Bragg reflections. The lower trace is a plot of the difference between calculated and observed intensities.

Fig. 2. Crystal structures of Ln_3MoO_7. (a): Structure at room temperature (space group: $P2_12_12_1$); (b): Structure of La_3MoO_7 at 460 K (space group: *Pnma*).

Fig. 3. (a) Powder X-ray diffraction profiles of La_3MoO_7 at 300 and 460 K. (b) The profiles in the low 2θ range ($15\ ^{o} \leq 2\theta \leq 40^{o}$).

Fig. 4. Structural phase transition temperatures of Ln_3MO_7 (M = Mo, Ru, Re, Os, Ir) against the ionic radius of Ln^{3+} in eight-coordination.

Fig. 5. Temperature dependence of magnetic susceptibility for Gd_3MoO_7 at low temperatures. The inset shows the reciprocal susceptibility vs. temperature curve. The solid line is the Curie-Weiss fitting.

Fig. 6. (a) Temperature dependence of the specific heat divided by temperature (C_p/T) for Gd_3MoO_7. (b) Temperature dependences of the magnetic specific heat divided by temperature (C_{mag}/T) and the magnetic entropy change (S_{mag}) for Gd_3MoO_7.

Fig. 7. Temperature dependence of the magnetic susceptibility for Sm_3MoO_7 below 15 K.

Fig. 8. (a) Temperature dependence of the specific heat (C_p) for Sm_3MoO_7. (b) Temperature dependences of the magnetic specific heat divided by temperature (C_{mag}/T) and the magnetic entropy change (S_{mag}) for Sm_3MoO_7.

Table 1. Lattice and positional parameters for Gd_3MoO_7

	Site	*x*	*y*	*z*	*B* / Å^2
Space Group: $P2_12_12_1$		*a* = 7.4459(1) Å, *b* = 7.4840(1) Å, *c* = 10.5620(2) Å			
R_I = 2.26 %, R_{wp} = 9.91 %					
Gd(1)	4*a*	0.9801(2)	0.0100(5)	0.7573(6)	0.45(2)
Gd(2)	4*a*	0.7145(1)	0.7536(8)	0.5334(2)	0.45
Gd(3)	4*a*	0.6970(5)	0.7479(8)	0.9843(2)	0.45
Mo	4*a*	0.4955(5)	0.0020(8)	0.7518(8)	0.10(4)
O(1)	4*a*	0.574(2)	0.742(4)	0.763(2)	0.50(30)
O(2)	4*a*	0.782(3)	0.969(4)	0.143(2)	0.50
O(3)	4*a*	0.128(3)	0.048(4)	0.109(2)	0.50
O(4)	4*a*	0.832(3)	0.962(4)	0.388(2)	0.50
O(5)	4*a*	0.216(3)	0.034(4)	0.368(2)	0.50
O(6)	4*a*	0.960(3)	0.740(6)	0.879(3)	0.50
O(7)	4*a*	0.011(3)	0.771(5)	0.606(3)	0.50

Note: $R_{wp} = \left[\sum w\left(|F(o)| - |F(c)|\right)^2 / \sum w|F(o)|^2 \right]^{1/2}$ and

$R_I = \sum |I_k(o) - I_k(c)| / \sum I_k(o).$

Table 2. Lattice and positional parameters for La_3MoO_7

	Site	*x*	*y*	*z*	*B* / Å^2
300 K					
Space Group: $P2_12_12_1$		*a* = 7.6043(3) Å, *b* = 7.7225(4) Å, *c* = 11.1090(7) Å			
R_I = 1.83 %, R_{wp} = 9.18 %					
La(1)	4*a*	0.9801(2)	0.0078(5)	0.7555(6)	0.34(2)
La(2)	4*a*	0.6935(1)	0.7522(8)	0.5352(2)	0.34
La(3)	4*a*	0.6923(5)	0.7487(8)	0.9795(2)	0.34
Mo	4*a*	0.4960(5)	0.0018(8)	0.7496(8)	0.19(4)
O(1)	4*a*	0.571(2)	0.746(4)	0.760(2)	0.21(15)
O(2)	4*a*	0.799(3)	0.962(4)	0.132(2)	0.21
O(3)	4*a*	0.139(3)	0.049(4)	0.114(2)	0.21
O(4)	4*a*	0.825(3)	0.952(4)	0.382(2)	0.21
O(5)	4*a*	0.197(3)	0.048(4)	0.375(2)	0.21
O(6)	4*a*	0.970(3)	0.765(6)	0.885(3)	0.21
O(7)	4*a*	0.984(3)	0.770(5)	0.624(3)	0.21
460 K					
Space Group: *Pnma*		*a* = 7.7273(2) Å, *b* = 11.1406(3) Å, *c* = 7.5881(2) Å			
R_I = 2.31 %, R_{wp} = 12.06 %					
La(1)	4*c*	0.0030(9)	1/4	0.7590(6)	0.76(3)
La(2)	8*d*	0.2498(7)	0.4720(1)	0.4422(2)	0.76
Mo	4*c*	0.9965(13)	1/4	0.2486(9)	0.24(6)
O(1)	8*d*	0.974(4)	0.370(3)	0.433(4)	0.72(20)
O(2)	8*d*	0.945(4)	0.880(3)	0.922(4)	0.72
O(3)	8*d*	0.232(4)	0.384(1)	0.724(2)	0.72
O(4)	4*c*	0.263(7)	1/4	0.312(2)	0.72

Note: $R_{wp} = \left[\sum w\left(|F(o)| - |F(c)|\right)^2 / \sum w|F(o)|^2 \right]^{1/2}$ and

$R_I = \sum |I_k(o) - I_k(c)| / \sum I_k(o).$

Table 3 Crystal structures of Ln_3MO_7 at room temperature

Ln	Ln_3MoO_7	Ln_3NbO_7	Ln_3TaO_7	Ln_3SbO_7	Ln_3ReO_7	Ln_3OsO_7	Ln_3IrO_7	Ln_3RuO_7
La	$P2_12_12_1$	*Pnma*	*Cmcm*	*Cmcm*		*Cmcm*		*Cmcm*
Pr					*Cmcm*		*Cmcm*	
Nd			$C222_1$	$C222_1$				
Sm		$C222_1$						
Eu								
Gd								$P2_1nb$
Tb					$C222_1$			
Dy		*Fm*-3*m*						
Ho			*Fm*-3*m*					
Er								
Tm								
Yb								
Lu								

Note: A symbol } denotes that two phases coexist.

Table 4 Magnetic data for Ln_3MoO_7

	magnetic properties	μ_{eff} (μ_B)	θ (K)	Ref.
La_3MoO_7	magnetic anomaly at 150, 380 K			[28,30]
Ce_3MoO_7	paramagnetic	2.49	-155	[39]
Pr_3MoO_7	magnetic anomaly at 8.0 K	6.42	-79(1)	[30]
Nd_3MoO_7	antiferromagnetic, T_N = 2.5 K	6.46	-57.4(8)	[30]
Sm_3MoO_7	magnetic anomaly at 0.8, 2.5 K	*	*	this study
Eu_3MoO_7	paramagnetic	*	*	[30]
Gd_3MoO_7	antiferromagnetic, T_N = 1.9 K	14.06(2)	-7.4(1)	this study

* Sm^{3+} and Eu^{3+} ions show the van Vleck paramagnetism.

Table 5 Magnetic Properties of Ln_3MO_7

Ln	Ln_3MoO_7	Ln_3NbO_7	Ln_3TaO_7	Ln_3SbO_7	Ln_3ReO_7	Ln_3OsO_7	Ln_3IrO_7	Ln_3RuO_7
La	T_N = 150 K	_	dia	dia		T_N = 45 K		T_N = 18 K
Pr	anomaly at 8.0 K	para	para	para	spin-glass like at 10 K	-	para	T_N = 55 K
Nd	T_N = 2.5 K	T_N = 0.6, 2.6 K	T_N = 2.1, 2.6 K	T_N = 2.5, 3.0 K	long-range magnetic order at 9 K	T_C = 75 K	T_N = 2.6 K	T_N = 19 K
Sm	anomaly at 0.8, 2.5 K	para	para	para	T_N = 1.9 K	weak ferro T_C = 48 K	para	T_N = 10.5, 22.5 K
Eu	para	para	para	para	anomaly at 12 K	complex behavior at 50 K	para	T_N = 22.5 K
Gd	T_N = 1.9 K	para	para	T_N = 2.6 K	T_N = 7.0 K	ferro T_C = 34 K		T_N = 9.5, 15 K
Tb		T_N = 2.2, 3.9 K	T_N = 2.9, 3.6 K	T_N = 3.0 K	T_N = 14.0 K			
Dy		para	T_N = 2.3 K	T_N = 3.2 K	T_N = 2.8 K			
Ho		para	weak ferro T_N = 2.6 K	T_N = 2.2 K	para			
Er		para	para	para				
Tm		para	para	para				
Yb		para	para	para				
Lu		_	dia	dia				

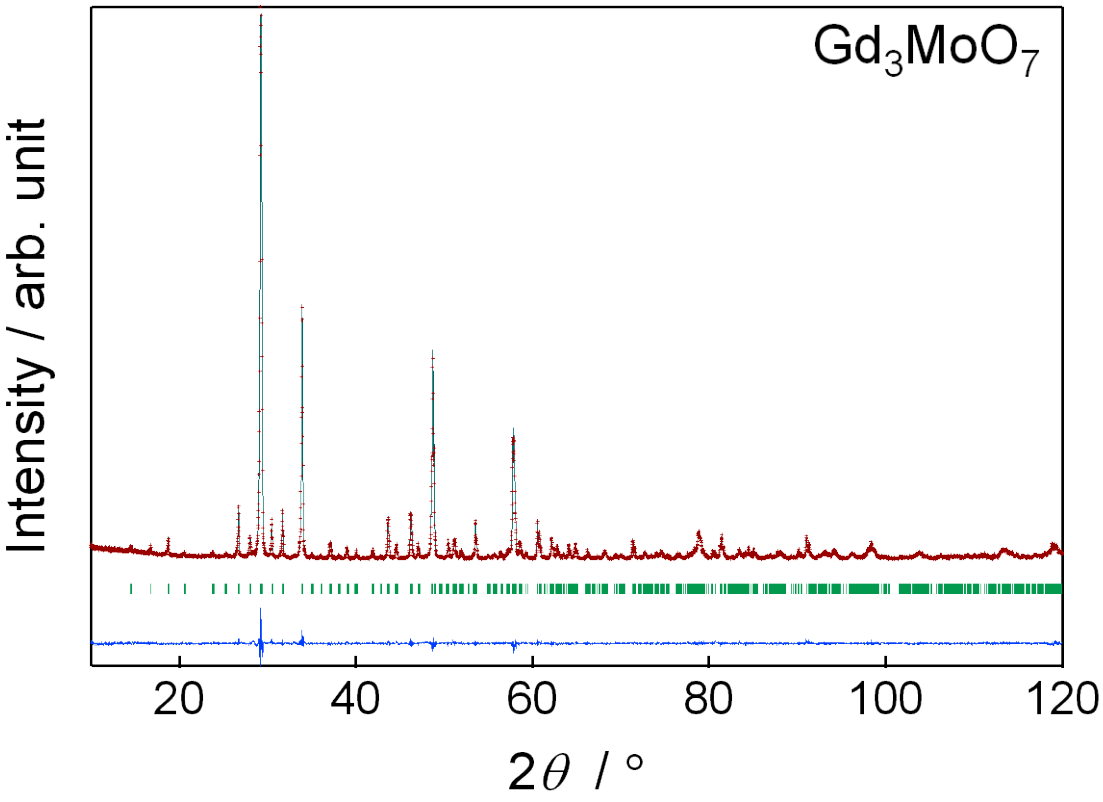

Fig. 1

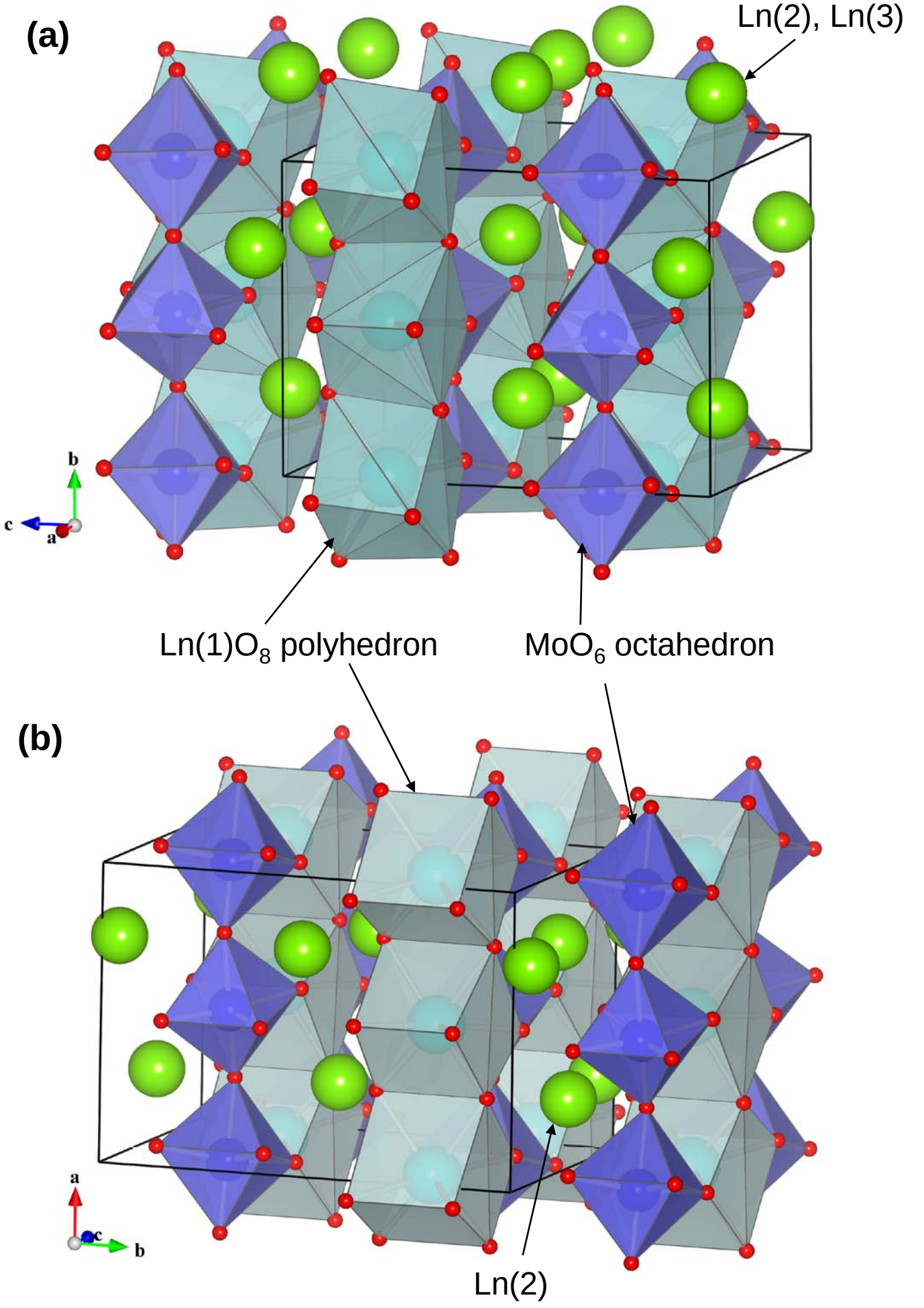
(a)
Ln(2), Ln(3)
b
c
a
Ln(1)O8 polyhedron
MoO6 octahedron
(b)
a
c
b
Ln(2)

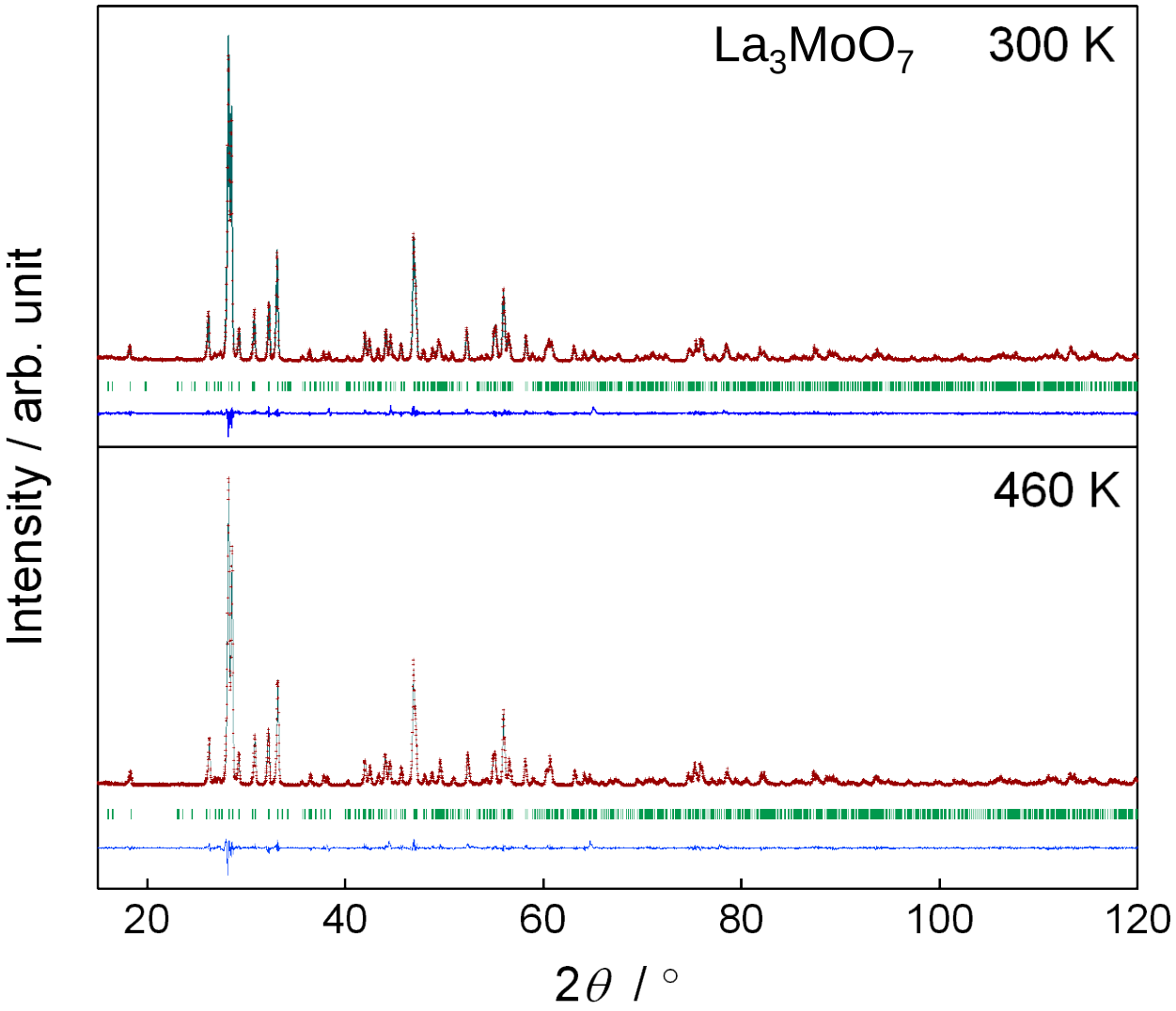

Fig. 3 (a)

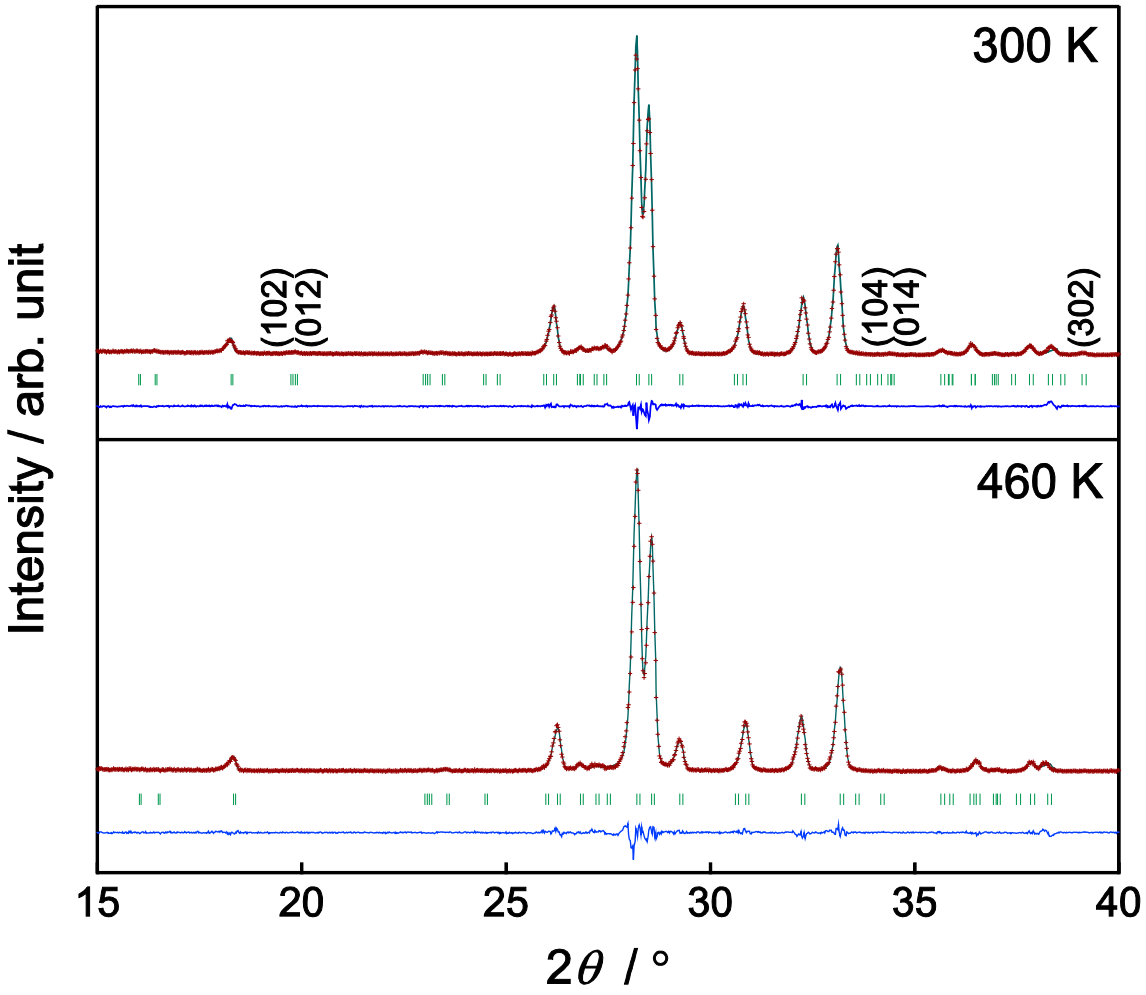
300 K
460 K
(102)
(012)
(104)
(014)
(302)
Intensity / arb. unit
15
20
25
30
35
40
2θ / °

Fig. 3(b)

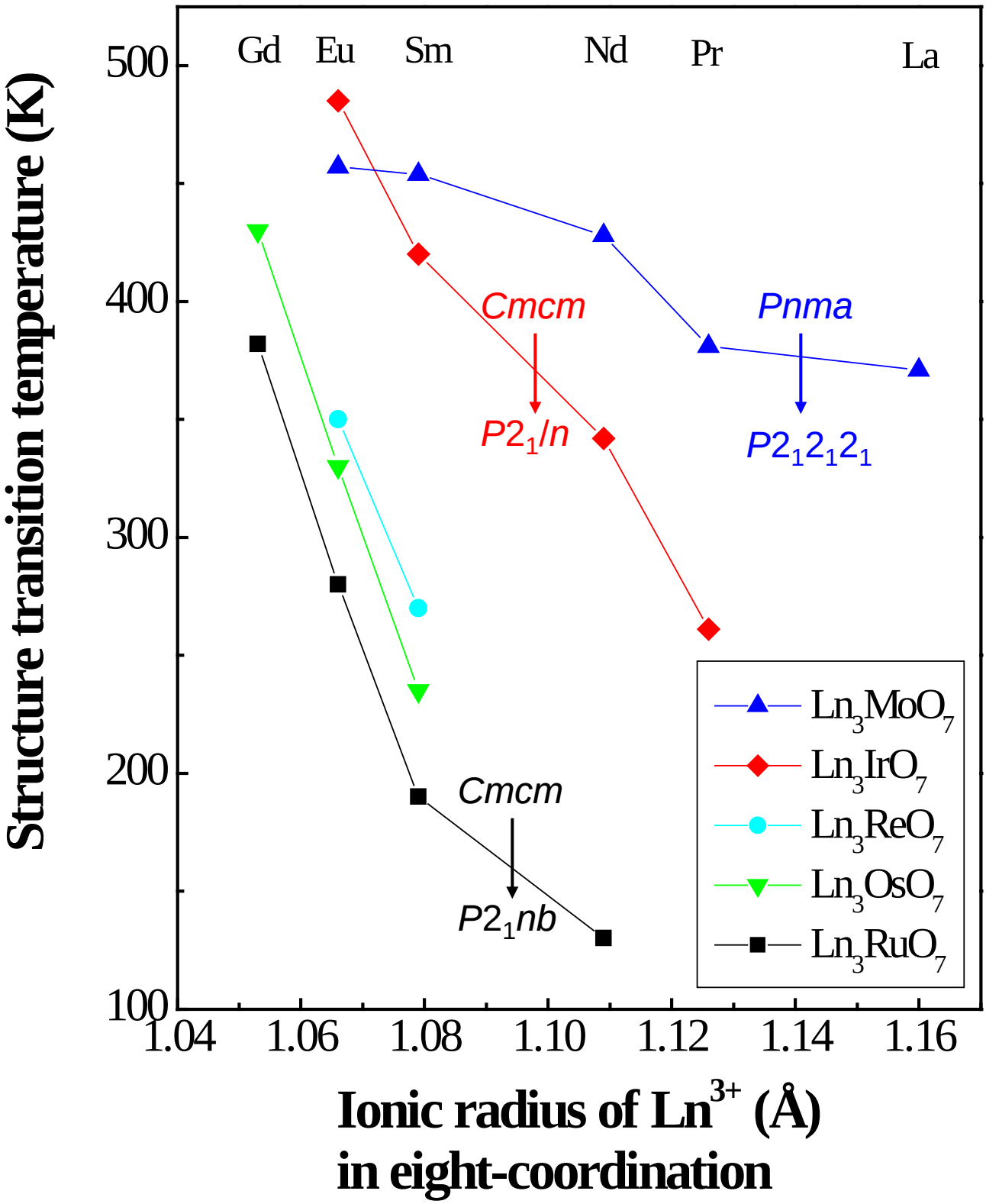
Gd
Eu
Sm
Nd
Pr
La
500
400
300
200
100
1.04
1.06
1.08
1.10
1.12
1.14
1.16
Structure transition temperature (K)
Ionic radius of Ln3+ (Å)
in eight-coordination
Cmcm
P21/n
Pnma
P212121
Cmcm
P21nb
Ln3MoO7
Ln3IrO7
Ln3ReO7
Ln3OsO7
Ln3RuO7

Fig. 4

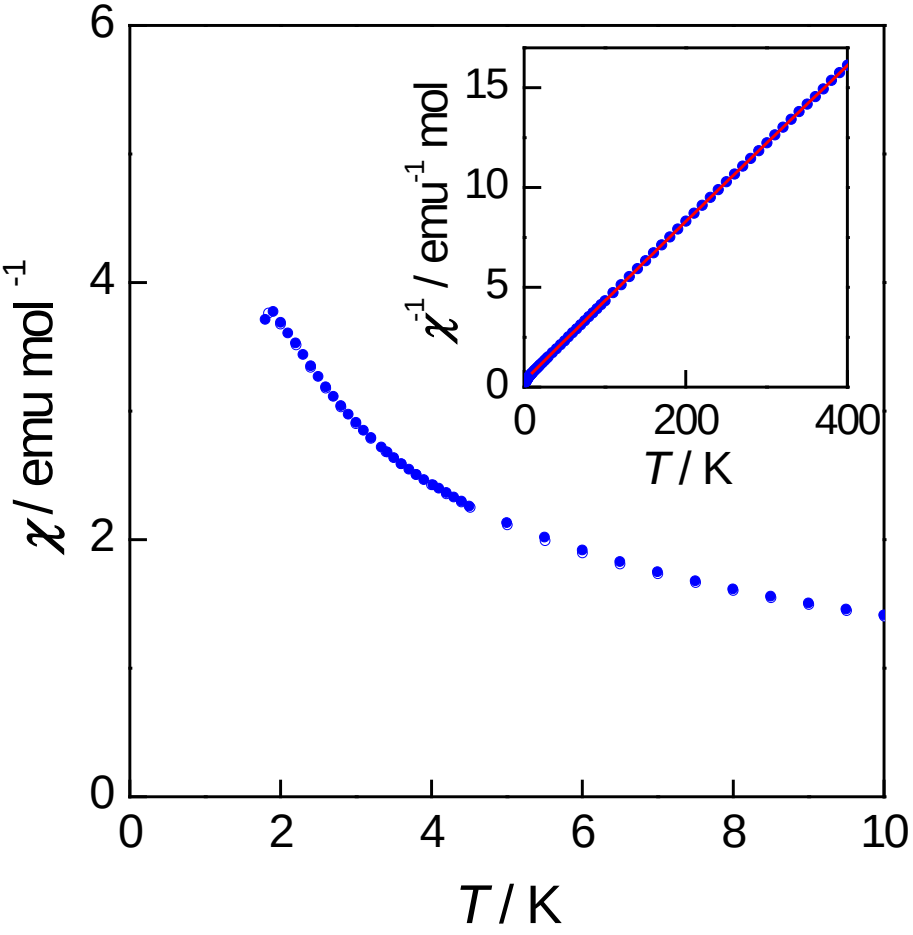

Fig. 5

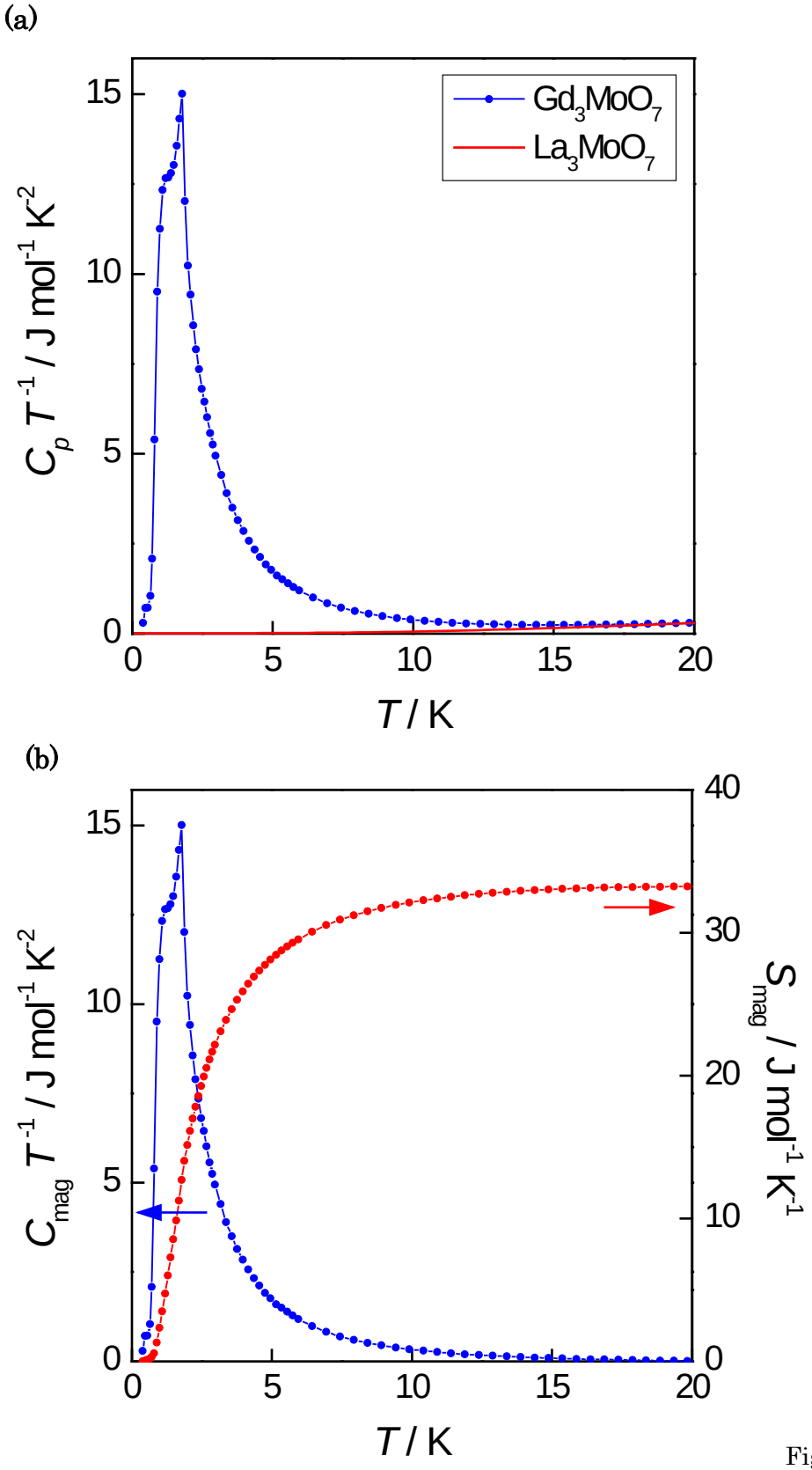
(a)
Gd3MoO7
La3MoO7
Cp T-1 / J mol-1 K-2
T / K
0
5
10
15
20
(b)
Cmag T-1 / J mol-1 K-2
Smag / J mol-1 K-1
T / K
0
5
10
15
20
30
40

Fig. 6

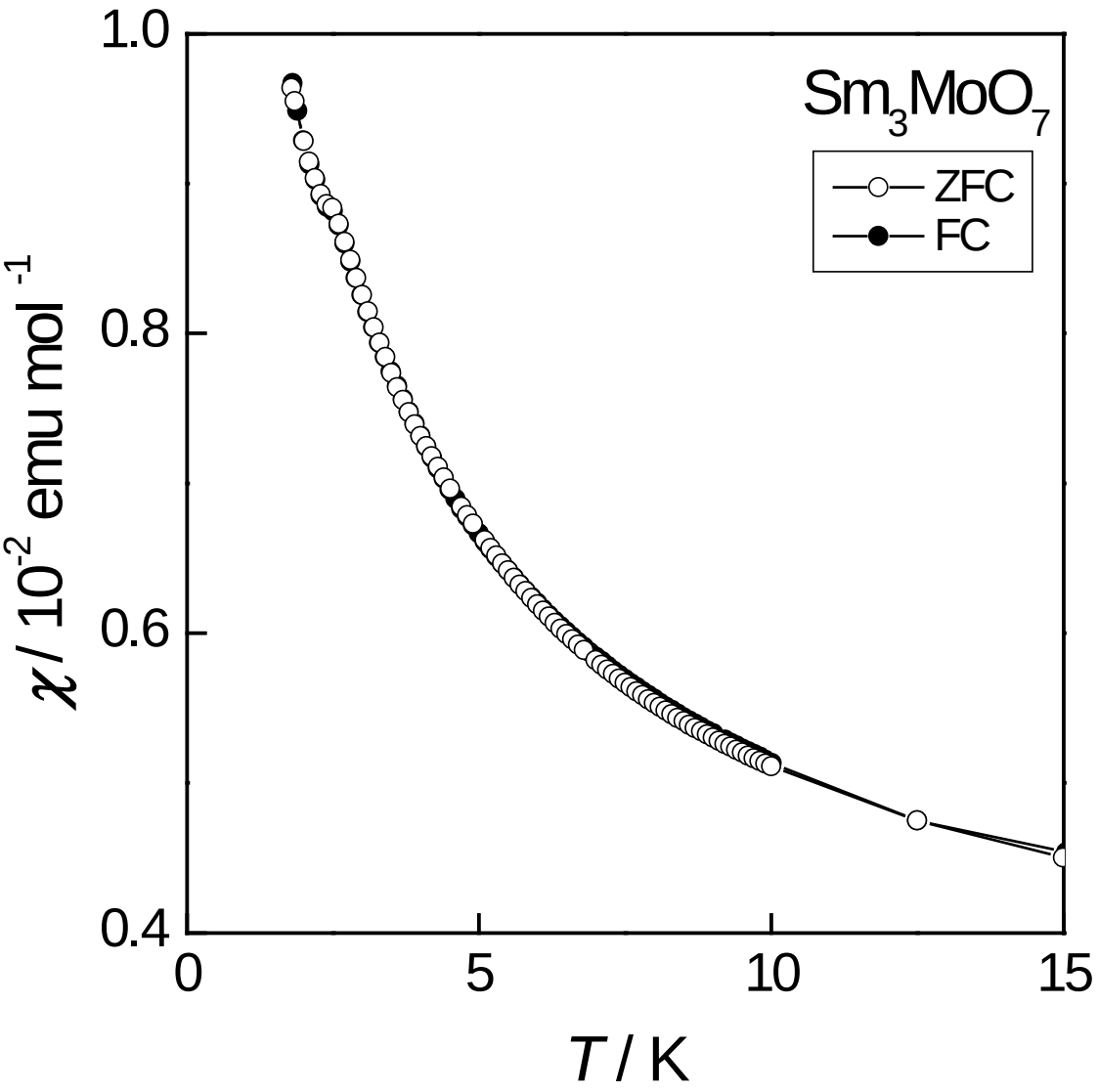

Fig. 7

(a)

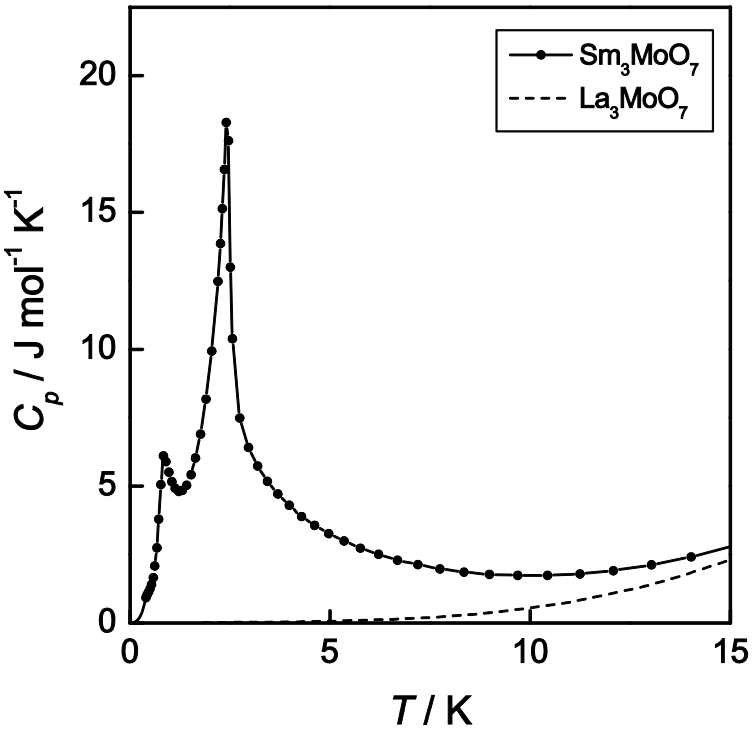
Sm3MoO7
La3MoO7
Cp / J mol-1 K-1
T / K
0
5
10
15
20

(b)

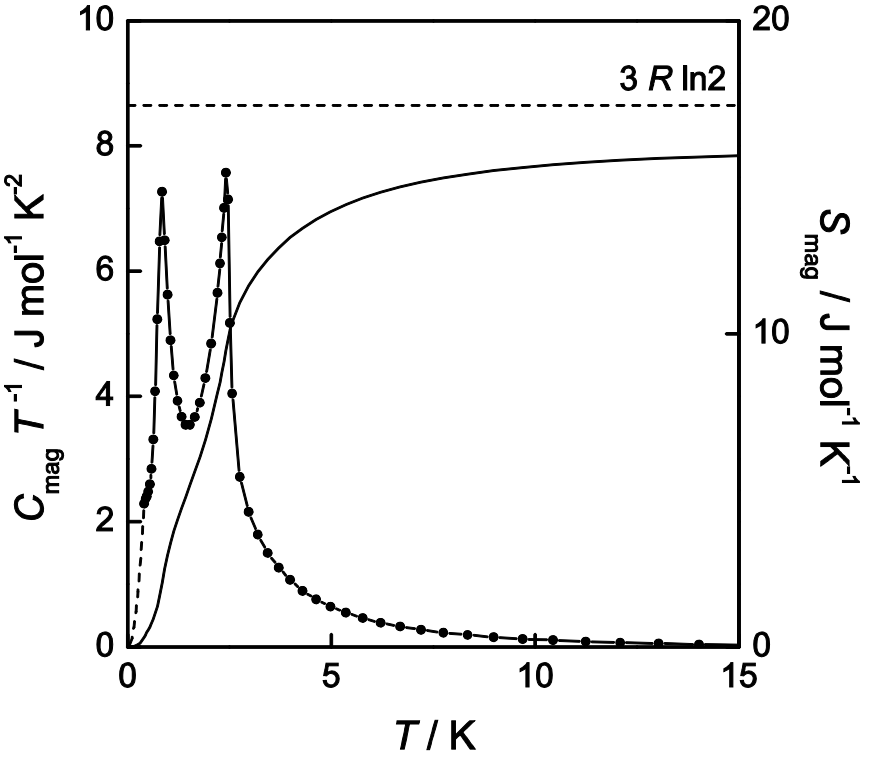
3 R ln2
Cmag T-1 / J mol-1 K-2
Smag / J mol-1 K-1
T / K
0
2
4
6
8
10
20

Fig.8